Formation of Porous Gas Hydrates from Ice Powders: Diffraction Experiments and Multistage Model

Doroteya K. Staykova,[†] Werner F. Kuhs,*[,†] Andrey N. Salamatin,[†,‡] and Thomas Hansen[§]

GZG Abt. Kristallographie, Georg-August-Universität Göttingen, Göttingen 37077, Germany, Department of Applied Mathematics, Kazan State University, Kazan 420008, Russia, and Institut Laue-Langevin, BP 156, F-38042 Grenoble Cedex 9, France

Received: December 20, 2002; In Final Form: June 24, 2003

Gas hydrates grown at gas−ice interfaces were examined by electron microscopy and found to have a submicron porous structure. In situ observations of the formation of porous CH_4- and CO_2-gas hydrates from deuterated ice Ih powders were made, using time-resolved neutron diffraction on the high-flux diffractometer D20 (ILL, Grenoble) at different pressures and temperatures. For the first time neutron diffraction experiments were also performed with methane in hydrogenated samples. The isotopic differences between H_2O and D_2O are found insignificant concerning the clathrate formation kinetics. At similar excess fugacities, the reaction of CO_2 was distinctly faster than that of CH_4. The transient formation of the CO_2-hydrate crystal structure II was also observed in coexistence with the usual type-I hydrate reaching a maximum of 5% after 5 h of the reaction at 272 K. A phenomenological model for the kinetics of the gas hydrate formation from ice powders is developed with special account of sample consolidation effects. It describes the initial stage (I) of hydrate film spreading over the ice surface and the two subsequent stages which are limited (II) by the clathration reaction at the ice−hydrate interface and (III) by the gas and water transport (diffusion) through the hydrate shells surrounding the shrinking ice cores. Comparable activation energies are found for stage II of the CH_4−hydrate formation in deuterated and hydrogenated ice with 8.1 and 9.5 kcal/mol, respectively. In the case of a diffusion-limited clathration (stage III) the activation energy in D_2O-ice powders can be estimated as 14.3 kcal/mol.

1. Introduction

Gas clathrate hydrates are nonstoichiometric inclusion compounds encaging small, usually apolar (guest) molecules in a framework of hydrogen bonded water (host) molecules. They exist as a stable solid phase at high gas pressures and/or low temperatures (van der Waals and Platteeuw, 1959).[43] Two main crystallographic structures of gas hydrates, von Stackelberg cubic structures I and II, are distinguished, both consisting of two types of cavities, small and large cages, that can be occupied by the guest molecules (Sloan, 1998).[32]

Since the 1950s, a large number of gas hydrate systems have been studied. Still, some physicochemical properties of gas hydrates as well as their formation and decomposition kinetics are neither well-known nor properly understood, though they are of primary importance for a number of reasons (Sloan, 1998).[32] With traces of water in gas and oil transport systems, hydrate stability conditions are met leading eventually to complete blockages of the pipelines. Likewise, the kinetics of CH_4-hydrate formation and decomposition is of major significance in geological settings, for our understanding of the role of methane gas in climate change, for the possible use of natural gas hydrate deposits as a future source of energy, or simply for a more economic transport and storage of gas. CO_2 clathrate hydrates could also be a possible form of sequestering CO_2 into the ocean to reduce global warming (Warzinski et al., 2000).[45] In the work presented here, we concentrate on studies of gas hydrate growth from ice. A strong dependence of the clathration reaction on the area of the gas-ice contact surface was demonstrated by Barrer and Edge (1967).[3] Later, Hwang et al. (1990)[14] studied the methane-hydrate growth on ice as an interfacial (heterogeneous) phenomenon and measured the clathrate formation rates during ice melting at different gas pressures. Sloan and Fleyfel (1991)[33] discussed molecular mechanisms of the hydrate-crystal nucleation on the ice surface, emphasising the role of the quasi-liquid layer (QLL). Takeya et al. (2000)[38] reported on the in situ observations of CO_2-hydrate growth from ice powder for various thermodynamic conditions using laboratory X-ray diffraction. They distinguished the initial ice-surface coverage stage and a subsequent stage which was assumed to be controlled by gas and water diffusion through the hydrate shells surrounding the ice grains. The process was modeled following Hondoh and Uchida (1992)[13] and Salamatin et al. (1998)[30] in a single ice particle approximation. The respective activation energies of the ice-to-hydrate conversion were estimated as 0.2 and 0.4 eV (4.6 and 9.2 kcal/mol). The first in situ neutron diffraction experiments on the kinetics of the clathrate formation from ice powders were presented by Henning et al. (2000).[11] They studied the CO_2-hydrate growth on D_2O ice Ih, using the high intensity powder diffractometer HIPD at Argonne National Laboratory for temperatures from 230 to 263 K at a gas pressure of approximately 900 psi (62 bar). The starting material was crushed and sieved ice. To interpret their results, the authors applied a simplified diffusion model of the flat hydrate-layer growth

* To whom correspondence should be addressed. E-mail: wkuhs1@gwdg.de.
[†] Georg-August-Universität Göttingen.
[‡] Kazan State University.
[§] Institut Laue-Langevin.

10.1021/jp027787v CCC: $25.00
Published on Web 08/26/2003

developed for the hydration of concrete grains (Fujii and Kondo, 1974;[10] Berliner et al., 1998[4]). The activation energy of 6.5 kcal/mol was determined for the later stage of the hydrate formation process. This work has been continued by Wang et al. (2002)[44] to study the kinetics of CH_4-hydrate formation on deuterated ice particles. A more sophisticated shrinking-ice-core model (Froment and Bischoff, 1990;[9] Levenspiel, 1999[23]) actually reduced to the diffusion model of Takeya et al. (2000, 2001)[38,39] has been used to fit the measurements. A much higher activation energy of 14.7 kcal/mol was deduced for the methane hydrate growth on ice. Based on Mizuno and Hanafusa (1987),[24] the authors suggested that the quasi-liquid layer of water molecules at the ice-hydrate interface may play a key role in the (diffusive) gas and water redistribution although a definite proof could not be given.

One of the recent and most intriguing findings is that, at least in certain cases (in abundance of guest species), some clathrate-hydrate crystals grow with a spongelike porous microstructure. Using cryo field-emission scanning electron microscopy (FE-SEM), direct observations of such submicron porous gas hydrates have now been made (Kuhs et al., 2000;[20] Klapproth, 2002;[17] Klapproth et al., 2002;[18] Staykova et al., 2002[34]). Hwang et al. (1990)[14] reported that the methane hydrates formed from ice in their experiments were very bulky and contained many voids. Optical microscopic investigations by Kobayashi et al. (2001)[19] also indicated a coarse and possibly porous microstructure of the hydrate films grown at liquid−liquid interfaces, especially in contact with flowing water. Rather interestingly, there are evidences that some natural gas hydrates from the ocean sea floor also exhibit submicron porosity (Suess et al., 2002).[36] Based on experimental studies (Aya et al., 1992;[2] Uchida and Kawabata, 1995;[42] Sugaya and Mori, 1996[37]) of CO_2 and fluorocarbon hydrate growth at liquid−liquid interfaces, Mori and Mochizuki (1997)[26] and Mori (1998)[25] had already proposed a porous microstructure of the hydrate layers intervening the two liquid phases and suggested a phenomenological capillary permeation model of water transport across the films. Although general physical concepts of this phenomenon in different situations may be quite similar, we still do not have sufficient data to develop a unified theoretical approach to its modeling (Mori, 1998).[25] The study presented here is confined to the particular thermodynamic conditions of gas hydrate formation from ice in a single-component gas atmosphere at pressures well exceeding the dissociation pressure at constant temperatures below the quadruple point.

In accordance with experimental observations (Uchida et al., 1992, 1994;[40,41] Stern et al., 1998;[35] Kuhs et al., 2000;[20] Henning et al., 2000;[11] Takeya et al., 2000;[38] Staykova et al., 2002[34]), a thin gas-hydrate film rapidly spreads over the ice surface at the initial stage I of the ice-to-hydrate conversion. Subsequently, the only possibility to maintain the clathration reaction is the transport of gas molecules through the intervening hydrate layer to the ice-hydrate interface and/or of water molecules from the ice core to the outer hydrate−gas interface. As mentioned above, a diffusion-limited clathrate growth was assumed and simulated by Takeya et al. (2000),[38] Henning et al. (2000),[11] and Wang et al. (2002)[44] on the basis of the shrinking-core models formulated for a single ice particle. However, in the case of porous gas hydrates, the gas and water mass transport through the hydrate layer becomes much easier, and the clathration reaction itself together with the gas and water transfer over the phase boundaries may be the rate-limiting step(s) at stage II of the hydrate formation that proceeds after the ice-grain coating (Salamatin and Kuhs, 2002).[31] Certainly, we can still expect the onset of a further stage III of the hydrate formation process completely or at least partly controlled by the gas and water diffusion through the clathrate phase, especially when a highly consolidated ice-hydrate structure develops with thick and dense hydrate shells surrounding ice cores.

The isotopic difference between H_2O and D_2O should also be emphasized. For instance, the water molecule mobilities in hydrogenated and deuterated ice Ih differ in terms of their dielectric relaxation, the deuterated compound having a somewhat longer relaxation time (Johari and Jones, 1976, 1978).[15,16] Although the role of water mobility in the clathration reaction or in gas and water mass transport is not clear, this indicates that the hydrate formation kinetics in the H_2O and D_2O systems may be different.

In the present study, we continue our previous work (Salamatin and Kuhs, 2002;[31] Staykova et al., 2002[34]) and attempt to quantitatively describe the formation process of CH_4 and CO_2 gas hydrates as followed by in situ neutron diffraction experiments starting from a well-characterized ice powder of known structure, grain size, and specific surface area. In addition to our kinetic diffraction studies, we present our ex-situ FE-SEM observations of the formation of porous gas hydrates which turned out to be very helpful to construct a phenomenological multi-staged model of gas-hydrate growth from ice powders. Special attention was paid to the hydrate-phase expansion beyond the initial ice-grain boundaries into the voids of the initial ice grain packing and the corresponding reduction of the specific surface of the hydrate shells exposed to the ambient gas. The model is then applied to fit and interpret the diffraction data of the formation process.

2. Experimental Section

Experimental Setup. We chose a neutron diffraction technique to investigate the gas hydrate formation kinetics because the strong penetration of neutrons permits the use of thick-walled high-pressure-gas equipment and cryogenic devices. In situ neutron diffraction experiments were performed at various pressures and temperatures with CH_4 and CO_2 gas on the high-intensity 2-axis neutron diffractometer D20 at ILL, Grenoble. D20 is a medium- to high-resolution diffractometer providing a very high flux at the sample position. It has 1536 detection cells of a stationary, curved linear position sensitive detector (PSD) covering a 2θ range of 153.6°. This makes D20 an ideal tool for in situ diffraction studies with acquisition times below 1 s allowing one to follow fast changes in the sample. More details about the instrument can be found at http://www.ill.fr/YellowBook/D20 and in Convert et al. (1998, 1999).[5,6]

Sample Preparation. Spherical ice Ih grains with a typical diameter of 40−80 μm were prepared (see Figure 1, parts a and b) in one batch in our laboratory at Göttingen using a spraying technique. The produced powder was collected and filled into thin-walled Al cans. For experiments with hydrogenated samples, special double-walled Al cans were manufactured in order to reduce sample absorption (because of the large incoherent cross section of hydrogen) at a maximum sample volume. The main characteristics of the ice samples are presented in Table 1.

To quantify the morphology of the starting material, a representative part of the sample was investigated by FE-SEM. The obtained pictures were used to estimate the size distribution of the ice spheres produced by the spraying techniques. Measurements on different batches showed that the size distribution of ice spheres sprayed with the same nozzle is well reproducible and has a log-normal shape. By using different

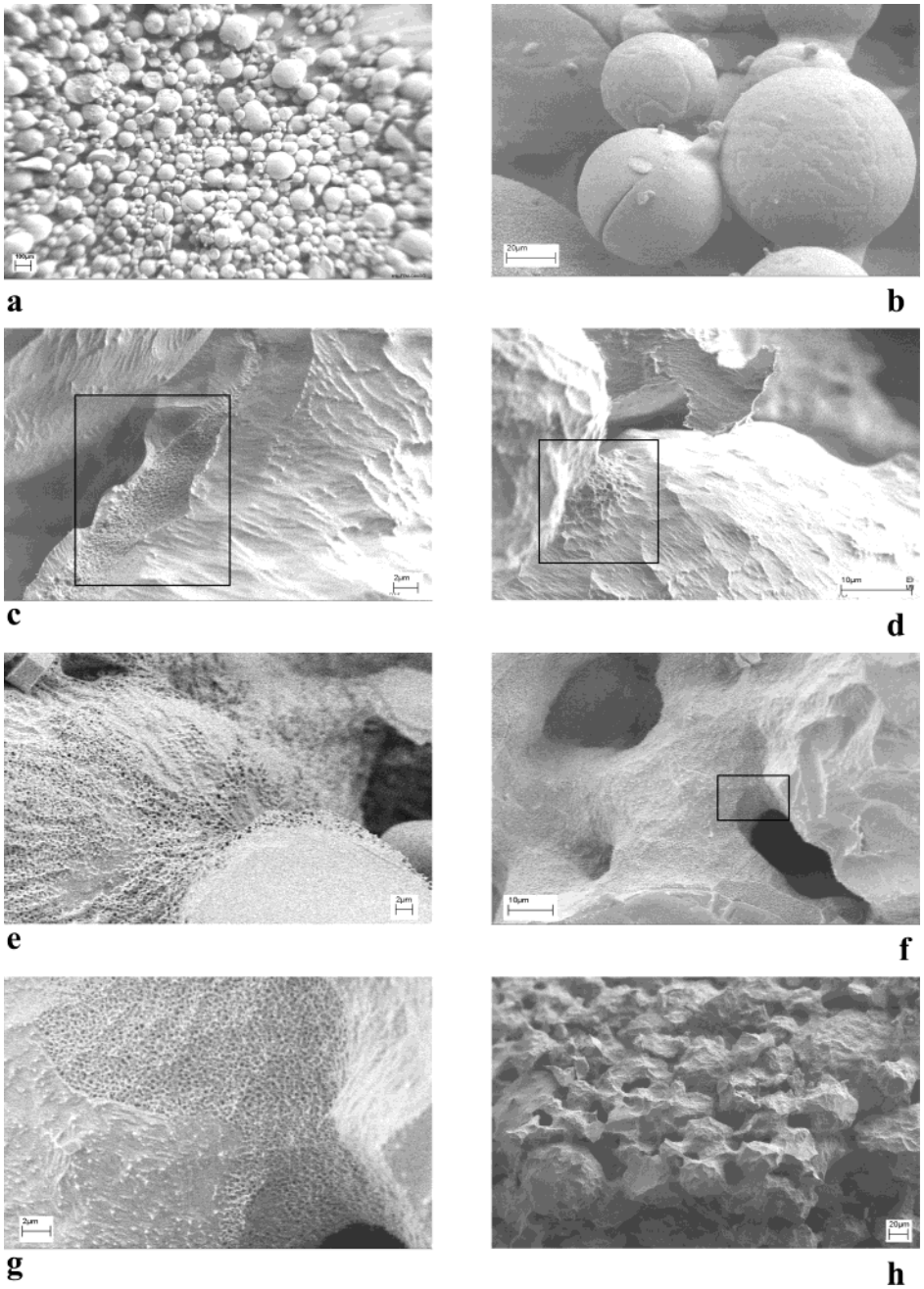

Figure 1. Field-emission scanning electron images of the starting ice-Ih material as well as samples quenched at various stages of the gas-hydrate formation process: (a) initial hydrogenated-ice-Ih powder; (b) ice spheres with average diameter of 40−60 μm seen at larger magnification of hereof; ice grain's crack (c) filled with the hydrate film and ice grains contact area (d) covered with a hydrate film after 1 h of reaction in H_2O-CH_4 system at 60 bar and 264 K; (e) split grain (lower right) and neighboring grain (left) with the surface covered by porous CH_4-hydrate after 10.5 h of reaction at 60 bar and 268 K; (f) D_2O-ice grains completely covered and sintered together by CH_4-hydrate after 55 h of reaction at 60 bar and 268 K; (g) larger magnification of the left-corner area from (f) showing the porous hydrate spreading into the open pore space of the initial ice sample; (h) Overview of a hydrate sample (H_2O-CH_4 system at 60b, 243 K, after 80 h of reaction) in which the original ice grain structure can still be discerned and showing a degree of sintering which leads to a macroscopically consolidated sample. Boxes on the images c, d, and f mark the regions of interest or magnification.

nozzles, we can produce samples with different particle size. For example, in the three series of our experiments described in Table 2, the mean diameters were about 77 and 55 μm. The estimated initial macroporosity of samples $\epsilon_{m0} \approx 30\%$ corresponds to the packing density of about 70%. Preliminary direct measurements of the specific surface area of the ice powder were performed on the basis of the gas adsorption method developed for the investigation of snow samples (Legagneux et al., 2002).[22] In this case for a mean grain size of about 80−100 μm, the obtained estimate of 750 cm^2/g (1.35 m^2/mol) is very close to the sum of the surface areas of single ice spheres as seen from the FE-SEM images. This supports the main assumption used in our model construction below that the contact areas and cracks do not significantly change the specific surface of the ice powder.

The Al cans with the prepared ice samples were transported in a dry-N_2 mover dewar to ILL/Grenoble. Two high strength auto-frettaged aluminum gas pressure cells were manufactured in Göttingen and adapted to an ILL sample stick. The sample temperature reading was obtained from a calibrated temperature sensor fixed to the pressure cell wall. The Al sample cans were inserted into the pressure cell, already fixed to the sample stick,

TABLE 1: Characteristics of Ice Samples and Gas Hydrates

parameters and denotations	values
ice samples	
ice density ρ_i, kmol/m^3	51
typical (mean) grain size r_{i0}, μm	25−40
specific surface area S_{i0}, m^2/mol	1.5−2.1
macroporosity ϵ_{m0}	0.33
coordination number Z_0	7
random density slope of particle distribution C	15.5
gas hydrates	
water density in hydrate phase ρ_{hw}, kmol/m^3	41.2
mesoporosity of CH_4 (CO_2) hydrates ϵ_h	0.15 (0.1)

and the Bridgman seal was closed. This filling operation was performed at an applied small stream of gas to ensure a complete filling of the system with the chosen gas. Subsequently, the pressure cell was inserted into the orange cryostat and the temperature was equilibrated at the chosen value. Then the wanted gas pressure was applied within a few seconds while the acquisition of data was started simultaneously. In our experiments, we did not observe any induction time; all reactions started immediately (within the diffractometer time resolution of a few seconds) after applying gas pressures higher than the decomposition pressure.

Acquisition and Processing of the Data. To observe the changes of the diffraction patterns during gas hydrate formation, we used D20 at its highest intensity setting for the wavelength of $\lambda = 2.414$ Å. The reaction of gas (at constant pressure and temperature) with ice grains was followed over a period of typically 10−20 h. The data were collected with a time resolution of 30 s or 1 min for the initial fast reaction and with a resolution of 5 min for the slower later part of the reaction in deuterated systems. In this case, data of a very good statistical precision were obtained suggesting that even time slices of 10 s would deliver useful information. In the experiments on hydrogenated systems, the quality of the measurements was considerably lower because of the inferior counting statistics and the higher background, and the reactions were followed in 10 min time slices only. Because of the lower sensitivity in the hydrogenated system, we did not obtain useful information for the first half hour of our experiments. All data were subjected to efficiency correction and background subtraction. Subsequently, the measurements were analyzed in an automated way with the use of the full-pattern Rietveld refinement program GSAS (Larson and Von Dreele, 1990)[21] delivering quantitative information on the amount of gas hydrate formed as a function of time with an accuracy of about 0.1% and 1.8% in deuterated and hydrogenated systems, respectively.

A two-phase (ice Ih + gas hydrate) Rietveld fit of the powder diffraction pattern obtained for each time slice was performed. Refined parameters were the lattice constants of ice Ih and gas hydrate, the phase fractions, and five background parameters; scale factor and absorption coefficient were fixed. The atomic positions and displacement parameters for D_2O (H_2O) ice Ih and CH_4- or CO_2-hydrate phases were taken from Klapproth (2002)[17] and were also kept fixed. The weight fraction of the clathrate phase α (mole fraction of ice converted to the gas hydrate) was extracted from the refinement for each time slice and plotted as a function of time.

FE-SEM Observations. Our previous (Kuhs et al., 2000;[20] Suess et al., 2002;[36] Staykova et al., 2002;[34] Klapproth, 2002;[17] Klapproth et al., 2002[18]) and recent ex situ FE-SEM observations of porous gas hydrates recovered at various stages of the formation process together with general physical and mechanical concepts allow us to formulate the following statements (which will be used to constrain a phenomenological model developed in the following paragraph to interpret our kinetic neutron diffraction experiments):

1. The starting material (ice Ih powder) consists of spherical grains of few tens to hundreds of μm in diameter (Figure 1, parts a and b). The arrangement of the ice grains in the sample is close to a random dense packing with a packing porosity of about 30%. The measured specific ice surface described above indicates minimum contact areas between grains.

2. The initial stage I of the ice grain surface coverage by a gas hydrate film is clearly distinguished from the subsequent stage(s) of the growth of the hydrate shell into the shrinking isolated ice cores. Different mechanisms are generally involved in the coating process such as (a) preferential filling of cracks in grains and necking between adjacent particles (Figures 1, parts c and d), (b) formation (nucleation) of hydrate patches on the ice surface, and (c) their lateral spreading (Figure 1e). Subsequently the porous gas-hydrate structure covers largely the ice surface (Figure 1, parts f−g) leading to a consolidated sample in which, however, the original ice grain structure can still be recognized (Figure 1h). Stage II is thought to be limited by the clathration reaction (including the gas and water redistribution across the phase boundaries), whereas stage III is assumed to be influenced (or fully controlled) by the water- and gas-mass transport through the hydrate layers from and to the inner parts of the original ice grains, respectively.

3. All our FE-SEM pictures show that the hydrate crystallites grown from ice are rather small (from a few to some tens of μm). Typically, single crystals of hydrates have an isotropic spongelike structure (see Figure 2) with the mean size of the pores in the order of several hundred nm for CH_4-, Ar-, and N_2-hydrate (*macropores* in the generally accepted terminology of porous materials) and several 10 nm for CO_2-hydrate (*mesopores* in this terminology). There is no obvious dependency of the pore size on pressure and temperature nor on the time of reaction. The internal meso- to macroporosity of the

TABLE 2: Conditions of Experiments and Kinetic Parameters of Gas-Hydrate Formation

	conditions of experiments							parameters of reaction-(diffusion-) limited kinetics[a]				
series no.	ice	r_{i0}, μm	gas	T, K	$p(f)$, bar	$p_d(f_d)$, bar	duration, h	ω_S, 1/h	A	B, 1/h	D, m^2/h	d_0, μm
1	D_2O	38.5	CO_2	272	20(19.7)	11.4(11.3)	18	0.55	0.11 (−)	0.0077 (>0.1)	$>10^{-10}$ (4.5×10^{-12})	6.6 (5.7)
			CH_4		35(32.2)	24(22.6)	23	0.5	0.031 (−)	0.0013 (>0.03)	$>10^{-11}$ (4.0×10^{-13})	1.9 (1.6)
					60(52.1)	24(22.6)	18	0.5	0.039 (−)	0.0022 (>0.05)	$>10^{-11}$ (3.7×10^{-13})	2.4 (1.9)
2	D_2O	27.5	CH_4	268	60(51.6)	21.6(20.6)	8	0.4	0.046 (−)	0.0030 (>0.06)	$>10^{-11}$ (3.4×10^{-13})	2.1 (1.4)
				230	35(30.2)	5.3(5.2)	11.5	0.15	0.012 (−)	0.00055 (>0.01)	$>10^{-13}$ (3.5×10^{-15})	0.62 (0.63)
				230	60(46.2)	5.3(5.2)	11	0.15	0.011 (−)	0.00055 (>0.01)	$>10^{-13}$ (3.3×10^{-15})	0.57 (0.53)
3	H_2O	27.5	CH_4	264	60(51.2)	19.4(18.4)	17.5			0.0030	$>10^{-11}$	
				253	60(49.9)	14.2(13.6)	23			0.0024	$>10^{-12}$	
				230	60(46.2)	5.3(5.2)	14			0.00054	$>10^{-13}$	

[a] Parameters are deduced (ω_S) from SEM observations or inferred (A, B, and D) by fitting the model to the measurements.

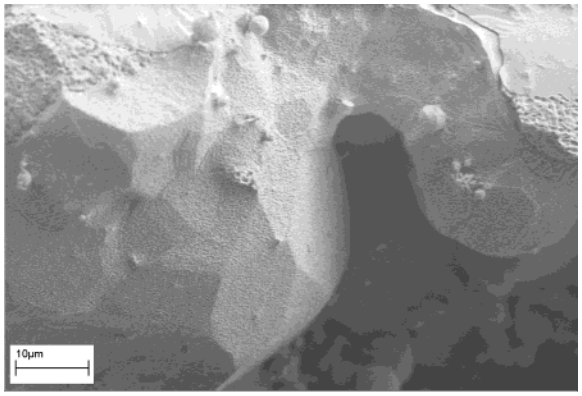

a

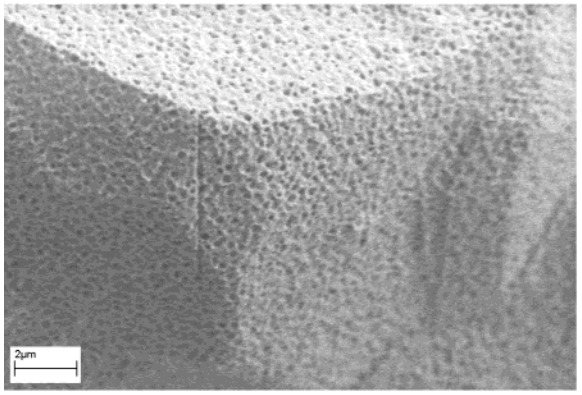

b

Figure 2. FE-SEM images of hydrogenated CH_4-gas hydrate obtained after 2 weeks of reaction at 60 bar 264 K. The gas-hydrate crystals with size of 20−30 μm show the faceting of crystallographic planes typical for a single crystal (a) and its clear submicron porous structure (b).

hydrate phase is visually estimated as 10−20% from the SEM photographs.

4. The diffraction data suggest a good crystallinity of the hydrate crystals, indicating a coherent "inward" growth of the hydrate shells without any appreciable deformation. This is also confirmed by the FE-SEM pictures which indicate that the growth process generally does not perturb the initial setting.

5. The density of water in the crystalline hydrate lattice of both types I and II is noticeably less than that of ice. Thus, the excess water molecules must be partly "evacuated" from the ice-hydrate contact area to vacate additional space for the newly formed porous clathrate hydrates. This water (∼20−30%) can be transported through the pore channels toward the outer hydrate surface to finally react with the ambient gas in the open space between the initial ice grains. Low-temperature specific surface area measurements show that some of the submicron pores in hydrates are open and their specific surface is at least more than 1 order of magnitude larger than that of the macropores in the original ice-grain structure. The higher the mean size of ice grains, the less complete is the degree of ice-to-hydrate transformation in a given time, indicating that thick hydrate layers lose some of their permeability and/or lead to the closure of the open voids between the original ice grains.

6. The typical time scales of the heat and mass transfer processes in the ice-powder samples are small (∼5−10 min). The temperature in the pressure cell in the thermostat is practically uniform, and all substances and energy are rapidly redistributed within the open space of the sample volume.

3. Theoretical Section

Model Description. Because a molecular picture of the clathrate formation process is lacking, the primary goal of this study was the development of a phenomenological mathematical description for the different stages of the clathration reaction to interpret the experimental kinetic data.

In our considerations, the geometry of the ice powder structure is described in a monosize (or monodisperse) approximation, in terms of the mean ice grain (core) radius r_i and the specific surface area of ice grains per mole of water molecules S_i (with r_{i0} and S_{i0} for their initial values); ρ_i is the molar density of ice. Some of the ice grains in a sample may be connected by bonds. Nevertheless, in accordance with our observations, we assume that S_{i0} is equal to the sum of the spherical grain surfaces and by definition

$$r_i = r_{i0}(1-\alpha)^{1/3}, \quad S_i = S_{i0}(1-\alpha)^{2/3}, \quad S_{i0} = 3/(r_{i0}\rho_i) \qquad (1)$$

where α designates the total degree of the reaction (the mole fraction of ice converted to hydrate phase) which is the principal characteristic of the hydrate formation process developing in time t.

Furthermore, we introduce ω_S and ω_V to denote the rates of the ice surface coating and the subsequent volume ice-to-hydrate transformation, respectively. The former quantity can be defined as the fraction of the open (exposed to the ambient gas) ice surface which becomes covered by the initial hydrate film during a unit time period, whereas the latter one is the number of ice moles transformed to hydrate phase per unit of time on a unit area of ice surface after its coating.

We designate as δ_0 the thickness of the ice layer converted in the coating process to the initial hydrate film of thickness d_0. Parameter δ_0 (and d_0) is small compared to the mean grain size r_{i0}, whereas the rate of the initial hydrate film formation is assumed to be much higher than that of the hydrate layer growth on the coated surface ($\omega_S \gg S_{i0}\omega_V$). Thus, the ice surface area remains practically constant ($S_i \approx S_{i0}$) during stage I.

Consequently, in accordance with Salamatin and Kuhs (2002),[31] the degree of the ice-to-hydrate conversion in the sample is governed by the following mass balance equation:

$$\frac{d\alpha}{dt} = S_i[\rho_i\delta_0\omega_S e^{-\omega_S t} + \omega_V(1-e^{-\omega_S t})] \qquad (2)$$

A more general approach taking account of nonuniform local changes in thickness of the hydrate-film patches during the ice grain coverage stage was discussed in Salamatin and Kuhs (2002).[31] It was shown that the formulation of the principal kinetic equation in the form of eq 2 is well established under the assumptions stated above.

The driving force of the hydrate formation is the supersaturation of the gas−ice−hydrate system, $\ln(f/f_d)$, expressed via fugacities f and f_d of the gaseous phase at the imposed and decomposition pressures p and p_d at a given temperature T. For each stage, this driving force determines the clathration kinetics and is contributing to the different steps of the ice-to-hydrate conversion in proportion to their apparent resistances, namely, k_S^{-1} for the initial hydrate film spreading over the ice surface, k_R^{-1} and k_D^{-1} for the clathration reaction and gas/water permeation through the hydrate layer, respectively.

Hence, we conventionally write

$$\omega_S = k_S \ln\frac{f}{f_d}, \quad \omega_V = \frac{k_R k_D}{k_R + k_D}\ln\frac{f}{f_d} \qquad (3)$$

Depending on the rate-limiting step of the hydrate formation

process, ω_V describes either the rate of the clathration reaction (ω_R) in stage II when $k_D \gg k_R$ or the rate of the gas and water mass transfer through the hydrate shell (ω_D) in stage III when $k_D \ll k_R$. For comparable values of k_R and k_D in the second equation in eqs 3, both steps of the hydrate formation are simultaneously important.

Assuming an Arrhenius-type behavior of the clathration rate constants as a function of temperature, we write the following possible approximations:

$$k_J = k_J^* \exp\left[\frac{Q_J}{R_g}\left(\frac{1}{T^*} - \frac{1}{T}\right)\right], \quad J = \text{S, R, D} \tag{4}$$

where k_J^* and Q_J are the clathration rate constant at the reference temperature T^* and the activation energy of the J-type step; R_g is the gas constant.

In the following discussion, the phenomenological model 1−4 will be considered as a theoretical basis for the detailed analysis of the different stages of hydrate formation and will be used in the interpretation of the neutron diffraction data. Actually, each Jth step explicitly presented in the model may be divided into a sequence of sub-steps characterized by their own resistances the sum of which is k_J^{-1}. Nevertheless, for a fixed temperature, k_S and k_R can still be used as tuning parameters, but the permeation rate constant k_D depends on geometrical characteristics of the hydrate layers surrounding the ice cores and must be additionally specified as a function of α to complete eqs 2 and 3.

Permeation Resistance of the Hydrate Layer. Here we follow the geometrical description of the powder particle growth developed by Arzt (1982)[1] for a random dense packing of monodisperse spheres on the basis of the concept of Voronoi cells associated with the initial powder structure. The build-up of the starting material is characterized by the average number of contacts per particle (coordination number) Z_0 and the relative slope C of the random packing density function. Experimental estimates for these parameters deduced by Arzt (1982)[1] are given in Table 1.

As shown schematically in Figure 3a, the shape of each hydrate layer formed from a single spherical ice grain is represented as a truncated sphere of radius r_h. The ice core shrinks, and its radius r_i decreases because of the inward growth of the hydrate layer. However, because of the lesser density of water in the porous hydrate phase, the excess water molecules must be transported to the outward hydrate surface exposed to the ambient gas, and the hydrate layer simultaneously expands into the open space between the original ice grains. The existing contact areas between neighboring hydrate shells (ice-hydrate particles) increase, and additional contacts are formed as r_h grows. Correspondingly, the fraction s of the free hydrate surface area exposed to the ambient gas, the specific surface area of macro-voids S_m, and the macro-porosity of the sample ϵ_m decrease. This scenario of hydrate phase development is illustrated by Figure 3b.

The current sample geometry is related to the reaction degree α by means of the hydrate-volume expansion factor (for details see the Appendix):

$$E = \frac{\rho_i}{\rho_{hw}(1 - \epsilon_h)} - 1$$

where ρ_{hw} and ϵ_h are, respectively, the mole density of water and the mesoporosity in the clathrate phase (see Table 1). Accordingly, the initial hydrate film thickness is $d_0 = \delta_0(1 + E)$.

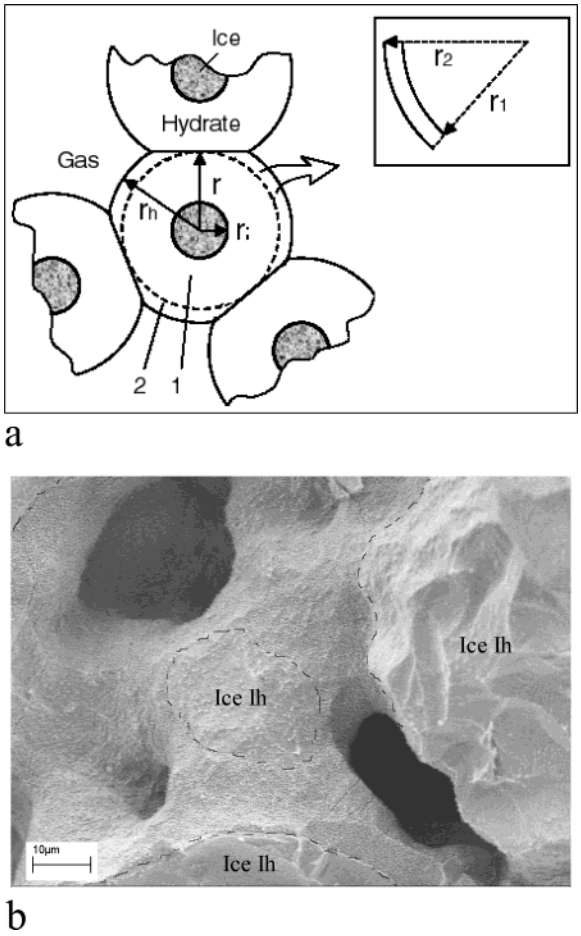

Figure 3. Gas-hydrate expansion into the open pore space of the ice sample. (a) A schematic of hydrate shell growth around a shrinking ice core. In the diffusion model (eq 5) the permeation resistance of the convex truncated sublayer 2 surrounding the inner spherical hydrate layer 1 is assumed to be similar to that of the concave spherical layer shown in the insert. See notations in text. (b) Extended FE-SEM picture of the CH_4-D_2O hydrate sample from Figure 1f. It reveals the pore closure process and shows (below) a cleaved grain with clearly distinguished boundary between the ice and the hydrate shell.

The fictitious spherical boundary of radius r in Figure 3a divides the hydrate shell into two sublayers 1 and 2: from r_i to r and from r to r_h, respectively. The permeation (diffusion) resistance of the spherical sublayer 1 is known from the diffusion theory (Crank, 1975).[7] To estimate the resistance of the truncated sublayer 2, we assume that locally the mass transfer process in the layer is similar to diffusion through a concave spherical layer of the same thickness with the same total areas of bounding surfaces (see the insert in Figure 3a). Finally, as explained in the Appendix, we arrive at the following relation for the permeation rate constant in eq 3:

$$k_D = \frac{\rho_i D}{r_{i0}}\sigma, \quad \sigma = \frac{\sqrt{s}R_h R}{R_i[\sqrt{s}R_h(R - R_i) + R_i(R_h - R)]} \tag{5}$$

Here D is the apparent gas/water mass transfer (permeation) coefficient (e.g., see Salamatin et al., 1998)[30] and σ is the complex geometrical characteristic of the developing sample structure expressed via normalized parameters $R = r/r_{i0}$, $R_i = r_i/r_{i0}$, and $R_h = r_h/r_{i0}$. The temperature dependence of the permeation coefficient follows eq 4 with k_D^* corresponding to D^* at the reference temperature T^* in eq 5.

If the expansion effect is neglected ($E = 0$), the hydrate shells in the sample remain within the initial ice-grain boundaries, R_h

and *s* equal unity, and eq 5 is reduced to the diffusive shrinking-core model for a single particle employed by Takeya et al. (2000)[38] and Wang et al. (2002).[44] Actually, in the case of a dense packing of the ice powder, such an approximation might be valid (see the Appendix) only in the very beginning of the hydrate formation process, at small α. However, $\sigma \rightarrow \infty$ (i.e., $k_D \rightarrow \infty$) in eq 5 when α and $R_h - R_i \rightarrow 0$ and, in accordance with eqs 2 and 3, the kinetics of the ice-to-hydrate conversion passes, at least shortly, through stages I and II controlled by the ice surface coverage process and/or by the clathration reaction, and not by the diffusion.

Qualitative Analysis of the Model. The solution of the general model 1−5 can be obtained only numerically. However, for fixed pressure and temperature conditions, during stages I and II, at least in the beginning of the clathration reaction when $k_D \gg k_R$, both quantities ω_S and ω_V given by eq 3 should be considered as constant values ($\omega_V = \omega_R$) and eq 2 can be integrated analytically. This asymptotic solution at $k_D \rightarrow \infty$ was derived and discussed in Salamatin and Kuhs (2002).[31] It takes the following form:

$$(1 - \alpha)^{1/3} = 1 - A(1 - e^{-\omega_S t}) - Bt \qquad (6)$$

where

$$A = \frac{\delta_0}{r_{i0}} - \frac{B}{\omega_S}, \quad B = \frac{\omega_R}{r_{i0}\rho_i}$$

It should be noted that parameter *A* is the difference of two small terms and, hence, its absolute value is expected to be small although the quantity itself can be both positive or negative.

Eq 6 requires that the plot of $r_i/r_{i0} = (1 - \alpha)^{1/3}$ against time *t* during stage II of the hydrate formation limited by the clathration reaction for $t \gg \omega_S^{-1}$ (after ∼5−15 h, see section 4 and Table 2) should be a straight line with slope *B* and intercept $1 - A$

$$(1 - \alpha)^{1/3} = 1 - A - Bt \qquad (7)$$

Parameter ω_S in eq 6 is determined by the curvature of the reaction degree graph at the initial stage I of the ice-surface coating. Parameters δ_0 (or d_0) and ω_R can easily be expressed via *A* and *B*, provided that r_{i0} (and *E*) is known. The *B* slopes and ω_S deduced at different temperatures directly result in estimates of the activation energies Q_R and Q_S in eq 4.

In the general case, the rate of the hydrate phase growth ω_V in eqs 2 and 3 after substitution of eq 5 can be given as

$$\omega_V = \omega_R\left(1 - \frac{1}{1 + F\sigma}\right), \quad F = \frac{D\rho_i}{r_{i0}k_R} \qquad (8)$$

The dimensionless complex *F* in eq 8 is the principal parameter responsible for the onset of stage III controlled (or influenced) by the gas/water mass transfer through hydrate shells surrounding the shrinking ice cores. As explained, the normalized factor σ changes from infinitely large values in the beginning of the clathration reaction to the first order of magnitude in the later phase of the gas-hydrate formation. Thus, the ice-hydrate system can never pass to the stage III at large *F*, and $\omega_V \approx \omega_R$ in eqs 3 and 8. For $F \ll 1$, stage II becomes extremely short and finishes together with stage I directly replaced by the diffusion-limited stage III. The intermediate values of $F \sim 1$ correspond to the onset of the stage III simultaneously controlled by both (reaction and diffusion) steps.

In the case of the hydrate formation process influenced by the gas and water transport through the hydrate layers the time behavior of the quantity $(1 - \alpha)^{1/3}$ becomes nonlinear. Correspondingly, after some time t^* in the beginning of the diffusion-limited stage III described (for small α) by the simplified diffusion theory of Fujii and Kondo (1974),[10] the relative ice-core radius r_i/r_{i0} is proportional to $(t - t^*)^{1/2}$. More elaborated models (Salamatin et al., 1998;[30] Takeya et al., 2000;[38] Wang et al., 2002[44]) predict even higher nonlinearity due to the decrease in the ice-core surface S_i. Still, they do not take into account the sample compaction and the reduction of the macropore surface S_m in the course of the ice-to-hydrate transformation as described by eq 5. The latter effects additionally suppress the gas and water fluxes through the hydrate shells to and from the ice cores and slow the reaction. Another peculiarity of the diffusion-limited conversion of ice powders to clathrate hydrates confirmed by eqs 1−3 and 5 is that the hydrate-growth rate in this case is inversely proportional to r_{i0}^2, being in contrast to the first two stages with *A* and *B* inversely proportional to r_{i0} in eq 6. Thus, the stages controlled by different rate-limiting steps (clathration reaction or gas/water transport through the hydrate shells) can be distinguished from each other. This may also help to recognize the formation of porous gas hydrates in the analysis of kinetic data.

4. Results and Discussion

Gas-Hydrate Formation Observed in Experiments. Two series of the in situ neutron diffraction experiments were performed with D_2O-ice and the third one with H_2O-ice. The only source of water molecules in the systems is ice, which reacts with gas and transforms to a clathrate phase. The gas-hydrate growth reveals itself by an increase of the Bragg intensities originating from the gas hydrates which starts immediately after the application of gas pressure and increases with time while the amount of ice Ih decreases. Repeatedly reported induction period (e.g., Sloan, 1998)[32] was not observed at our experimental conditions. The two sets of experiments performed with deuterated ice lasted between 8 and 23 h (Table 2). The temperature dependency of the CH_4 hydrate formation was evaluated in three runs at 230, 268, and 272 K (Figure 4a). The pressure influence is illustrated by runs performed at 60 and 35 bar for a temperature of 272 K (i.e., 4.7 K below the D_2O-ice melting point) and 230 K (Figure 4b). The kinetics of the formation of CH_4 and CO_2 hydrate are compared at 272 K (Figure 4c). It should be noted that the mean radius of the ice grains in the first set of experiments was larger (∼39 μm) than in other experimental series (∼28 μm). One short reaction (∼1.5 h) at 272 K and 60 bar (not included in Table 2) was additionally conducted to intercompare (see Figure 4d) the results obtained in the experiments with different initial ice particle size. In accordance with theoretical predictions, the reaction rates are noticeably higher for the sample with smaller grains. The enhancement factor of 1.4 (determined as the ratio of the degrees of reaction at a given time) is practically the same for all measurements. This observation is discussed and used for the data interpretation below.

In the third series (see Table 2), neutron diffraction experiments were performed starting from H_2O-ice powder in order to study the isotopic influence on the gas-hydrate formation process in deuterated and nondeuterated ice powders. Three experimental runs in H_2O-CH_4 systems at constant pressure of 60 bar and temperatures 230, 253, and 264 K were conducted for 14, 23, and 17.5 h, respectively. A typical kinetic curve obtained for the gas-hydrate growth from normal-water ice at

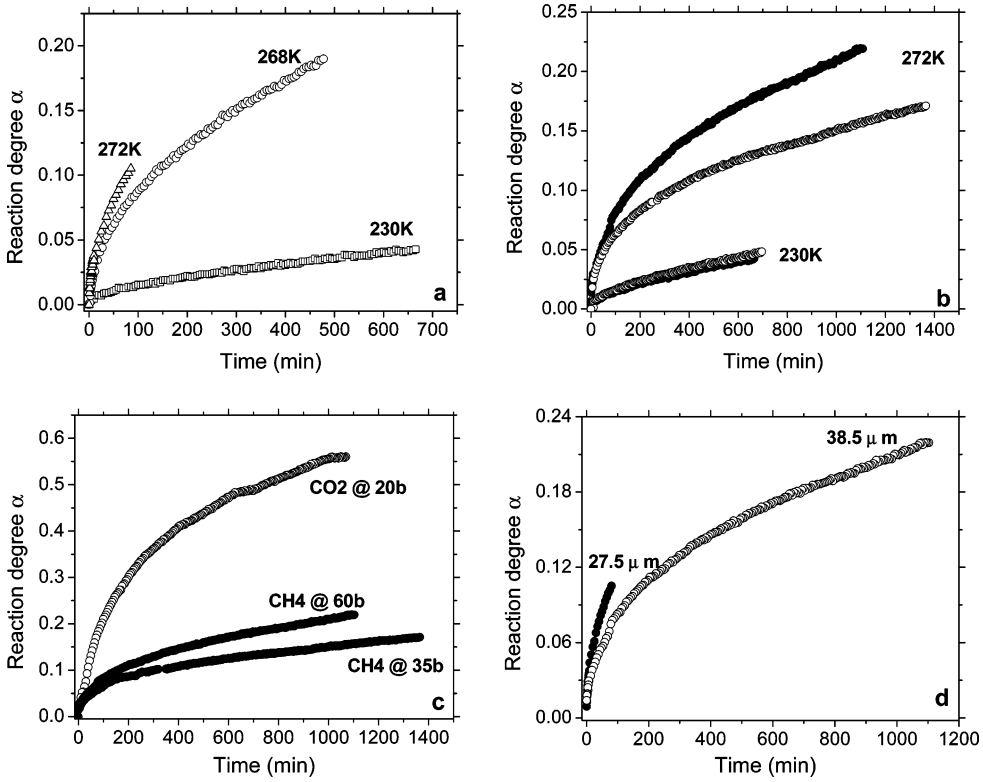

Figure 4. Temperature, pressure, and size dependency of the reaction kinetics. Each symbol shows a value of gas hydrate weight fraction obtained from one data file. (a) Temperature dependence of the clathration reaction of CH_4 with D_2O-ice at 60 bar. (b) Comparison of the hydrate growth rates in the CH_4-D_2O system at different pressures for 272 and 230 K. White and black circles correspond to 35 and 60 bar, respectively. (c) A comparison of the hydrate formation rates in case of CH_4 (35 and 60 bar) and CO_2 (20 bar) for 272 K. (d) Kinetic curves obtained for CH_4-D_2O system at identical thermodynamic conditions (60 bar and 272 K) in two experiments with different mean diameters of ice particles: 77 and 55 μm in short and long run, respectively. The reaction rate is inversely proportional to the grain size.

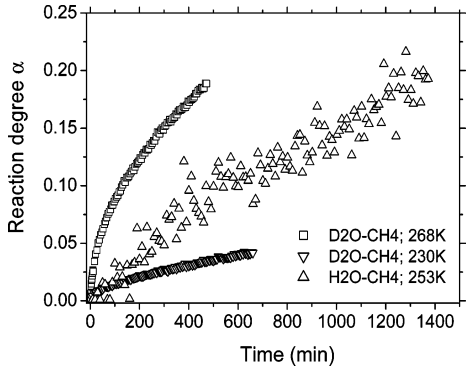

Figure 5. Comparison of the clathration rates in deuterated and hydrogenated methane systems at 60 bar for different temperatures.

253 K is compared with the heavy-water experiments at the same pressure and temperatures covering the range from 230 to 268 K in Figure 5.

The reactions in both systems showed no difference in their behavior. The data from the hydrogenated sample fall approximately in the middle between the curves obtained for deuterated ice. It indicates that the isotopic differences between H_2O and D_2O are probably insignificant in terms of their influence on the clathrate formation. If this is generally true, our experiments on deuterated samples can be considered as representative also for the hydrogenated case.

At high temperature the reduced (excess) fugacity $(f - f_d)/f_d$ clearly influences the rate of CH_4-hydrate formation (see Figure 4b and Table 2). It appears that at low temperature (at least in our experiments) this factor plays a minor role in the growth kinetics. The ice-to-hydrate conversion is definitely a temperature-dependent process (Figure 4a) with ~4% conversion occurring in 11 h and 22 and 15 min at 230, 268, and 272 K, respectively. In all runs for the initial stage, the kinetic curve reveals a strongly nonlinear development in time and flattens in the later stages. Our numerous electron microscopy observations of the porous hydrate layer during the stage I show that the coating process preferentially starts in cracks and at grain contacts (e.g., Figure 1, parts c and d), filling the cavities at 268 K within 1 h. It slows down subsequently, whereas formation and spreading of hydrate patches can be observed. Even at high temperatures the ice surface is not fully covered with a hydrate shell after several hours. As estimated from our SEM images, the duration of the stage I changes from a few hours to 1 day as temperature decreases from 272 to 230 K. The estimates of ω_S in Table 2 are based on these data.

A comparison of the data in Figure 4c shows a clear difference in the reaction kinetics of CH_4 and CO_2 gases. For example, the maximum conversion of ice into type-I gas hydrate at the end of the runs is 17% (22%) for CH_4 and 56% for CO_2 at respective excess fugacities of 0.42 (1.3) and 0.74. Thus, CO_2 reacts about 3 times faster than CH_4. It should also be noted that in the case of CO_2-clathrate growth, in accordance with earlier observations by Fleyfel and Devlin (1991),[8] the transient formation of a type II structure was observed (Figure 6). It should be noted that a type II hydrate structure has a higher proportion of small cages which seem to be preferred in the initial stages of the hydrate formation as evidenced in NMR work by Pietrass et al. (1995)[29] and Moudrakovski et al. (2001).[27] Some further discussion of this topic can be found in Klapproth et al. (2002).[18]

Model Investigation on CO_2-Hydrate Formation Kinetics. Let us apply the phenomenological model described in section

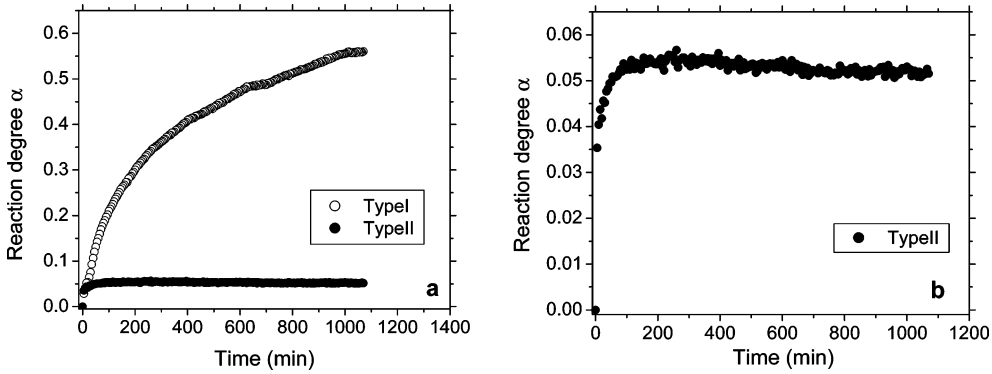

Figure 6. Simultaneous formation of a type I and type II structures of CO_2-hydrate plotted as phase fractions vs time (a). The development of structure II is shown in more detail on a plot b.

3 to interpret the neutron diffraction data on the gas-hydrate formation kinetics. An interactive computer program was developed to perform all necessary simulations. The most complete ice-to-hydrate conversion (up to 56%) was observed in the CO_2-D_2O clathration reaction (see Table 2 and Figure 4c). This makes the latter set of measurements especially valuable for a model validation and a comparison with numerical experiments. The main results of simulations in the case of the CO_2-hydrate growth from ice powders are shown in Figure 7. The principal conclusion is that the experimental kinetic curves can be equally well represented up to 60−70% of the conversion by both reaction- and diffusion-limited approximations (compare the best-fit curves 1 and 2 in Figure 7, parts a and b). Thus, in accordance with eq 8, only lower bounds for the reaction rate constant k_R (parameter B) at $F \rightarrow \infty$ or the mass transfer coefficient D at $F \rightarrow 0$ can be inferred in our study through the model constraining based on the available data. It is clear that a definite value of parameter A related to parameter B (see eq 6) can be deduced only for the hydrate formation process controlled by the clathration reaction. The corresponding best-fit estimates are gathered in Table 2. Actually, the difference in α between the two limiting cases (curves 1 and 2 in Figure 7a) is not essential even for higher values of the reaction degree. However, the diffusion-limited stage III manifests itself through the nonlinearity of the normalized ice-core radius variation versus time (compare the curves 1 and 2 in Figure 7b). Curve 3 in Figure 7b shows that this peculiarity becomes noticeably less prominent and would be underestimated by the model if the ice grains in the powder are considered separately as single spheres (Henning et al., 2000;[11] Takeya et al., 2000, 2001;[38,39] Wang et al., 2002[44]). The importance of the hydrate layer expansion during the reaction into the macropore space formed by the densely packed ice particles is also illustrated by considerable changes in the macro-porosity ϵ_m and specific surface area S_m of the sample depicted by curve 5 in Figure 7a and curve 1 in Figure 7c, respectively. Curve 2 in Figure 7c shows the corresponding growth of the normalized hydrate layer radius R_h.

As emphasized in section 3, the model predicts the hydrate formation rates to be differently sensitive to the mean initial grain size of the ice powder in the reaction- and diffusion-limited kinetics. The simulations (curves 3 and 4) performed for the two times larger particles (of 77 μm radius instead of 38.5 μm) fully confirm this peculiarity. In the beginning (during the stage II), for relatively small $\alpha < 0.2-0.3$ in eq 6, the hydrate growth rates controlled by reaction are inversely proportional to the mean particle radius, which accounts for the difference between the curves 1 and 3 in Figure 7a. In the case of the diffusion-limited process, the rates given by eqs 2, 3, and 5 decrease inversely to the mean radius squared. This is clearly seen from comparison of curves 2 and 4 in Figure 7a in the later period of the stage III. The dependence of the hydrate

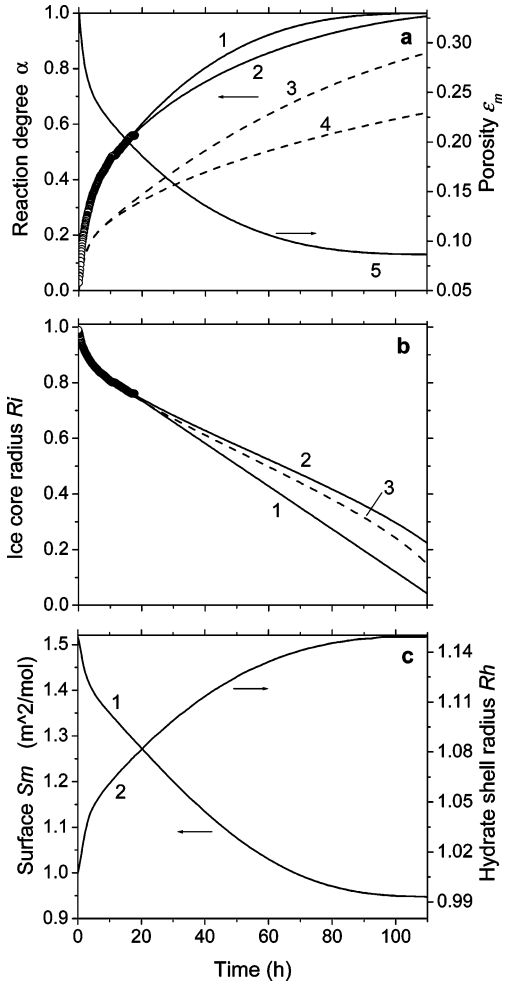

Figure 7. Simulated kinetic characteristics of the CO_2-hydrate growth from D_2O-ice powders at 20 bar and 272 K compared to the measurements (circles). (a) Reaction degree α (curves 1−4) and macro-porosity of samples ϵ_m (curve 5) vs time: curves 1 and 3 (2 and 4) are the reaction-limited (diffusion-limited) kinetics of hydrate formation from powders with mean grain radii of 38.5 and 77 μm depicted by solid and dashed lines, respectively; curve 5 corresponds to the reaction-limited case at $r_{i0} = 38.5$ μm. (b) The normalized mean radius of ice cores R_i vs time in the reaction-limited (curve 1) and diffusion-limited (curve 2) process for $r_{i0} = 38.5$ μm; curve 3 (dashed line) is the single shrinking ice-core model approximation. (c) Specific macropore surface area S_m (curve 1) and the normalized hydrate layer radius R_h (curve 2) vs time in the reaction-limited case at $r_{i0} = 38.5$ μm.

growth rates on the mean radius of ice grains can be used in experimental studies to distinguish the different rate-limiting steps of the gas-hydrate formation from ice powders. It should also be mentioned here that the model 1−5 assumes the starting material to be a monodispersed ice powder. Real samples in general should be considered as polydispersed systems. This would change the behavior of the simulated kinetic curve to even higher nonlinearity at a later phase of the reaction. Although not important at the present stage of our study, the latter effect should be introduced into the model in the future for interpreting the long-term experimental runs.

The inferred permeation coefficient of the gas and water mass transfer in CO_2-hydrate formed from deuterated ice powder 4.5 $\times$ 10^{-12} m^2/h at 272 K is in good agreement with the estimate of about 8 $\times$ 10^{-16} m^2/s (3 $\times$ 10^{-12} m^2/h) obtained by Takeya et al. (2000)[38] at 269 K for H_2O ice. This gives us additional evidence that the isotopic properties of ice do not significantly affect the gas-hydrate growth and the observed kinetics are similar. Unfortunately, the mean particle size in ice powders used by Henning et al. (2000)[11] was not reported and the comparison with their experimental data cannot be made.

The possibility of gas-hydrates being porous on the submicron level (Kuhs et al., 2000)[20] and the predominance of the reaction controlled stage II during the ice-to-hydrate conversion (Salamatin and Kuhs, 2002)[31] have not been considered in the kinetic studies so far. Hence, the estimates of the clathration reaction rate B inferred on the basis of eqs 6 and 7 and presented in Table 2 are the first available data. Simultaneously another parameter A is deduced through the model constraining. This gives the thickness of the initial hydrate layer, which spreads over the ice particle surface during the stage I. Both reaction- and diffusion-limited approximations lead to close estimates and in case of CO_2-hydrate formation $d_0 \sim 6-7$ μm using the best-fitting rate of ice coverage $\omega_S \approx 0.55$ h^{-1} at 272 K (see Table 2). It is interesting to mention that direct measurements performed by Ohmura et al. (2000)[28] with the use of laser interferometry gave the initial clathrate film thickness of about 10 μm on the liquid hydrofluorocarbon/liquid water interface after 6 h of reaction. It is somewhat intriguing that so similar dimensions of the initial hydrate layers are found in quite different systems, in liquid−liquid and gas−solid clathration reactions. Indeed, submicron porous gas hydrates are formed from both solid and liquid water, also pointing to closely related physicochemical processes on a nanometric scale.

CH_4-Hydrate Growth from Ice Powders. Although not so complete (with a total reaction degree not exceeding 10−22%), the diffraction kinetic measurements of the CH_4-hydrate growth from deuterated ice powders performed at different pressures and temperatures (see Figure 4) also present a valuable piece of information of rather high precision.

It is interesting to note that the ratio 1.4 between the reaction degrees in the two experiments in Figure 4d conducted at the same thermodynamic conditions equals the ratio between the initial mean grain radii of the ice samples. This observation is in full agreement with the computer simulations discussed in the previous section and indicates that, at least in the beginning, the formation of porous CH_4-hydrates is most likely controlled by the clathration reaction itself. However, the kinetic curves for the CH_4-D_2O system shown in Figure 4 can (as in the case of the CO_2-hydrate formation) be equally well fitted by the model predictions either for the reaction- or diffusion-limited process. Typically, in our simulations, the two limits are met at $F > 1-10$ and $F < 10^{-3}-10^{-2}$, respectively. Figure 8 gives

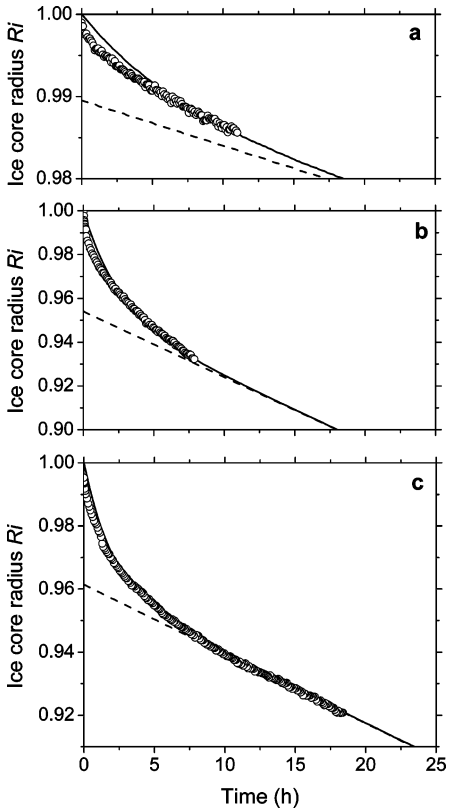

Figure 8. Model predictions (solid lines) fitted to the CH_4-hydrate formation data (circles) at 60 bar for 230, 268, and 272 K (plots a−c, respectively). The dashed lines correspond to eq 7 and show the transition of the stage I to the later stages II or III.

examples of the best fits found at 60 bar for 230, 268, and 272 K.

As explained above, the rates of the ice-surface coverage by the initial hydrate film ω_S for different thermodynamic conditions presented in Table 2 were estimated on the basis of SEM observations and noticeably decrease with temperature from $\omega_S \sim 0.5$ h^{-1} at 272 K to ~0.15 h^{-1} at 230 K. A relatively large scatter of the data in the experimental runs with H_2O ice and insufficient information about the initial parts of the kinetic curves (see section 2) for hydrogenated samples do not allow us to reliably constrain the model within stage I. Only the reaction rate slopes B can be determined. All model parameters inferred for the clathration reactions with methane are gathered in Table 2.

These results reveal a considerably lower thickness of the initial CH_4-hydrate layer coating the ice surface than in case of the CO_2-hydrate growth decreasing with temperature from $d_0 \sim 1.9-2.4$ μm at 272 K to 0.5−0.6 μm at 230 K. For the first time, the deduced estimates of the reaction rate slopes B, conceptually based on the evidence of a submicron porous microstructure of gas hydrates, can be used to determine the activation rate Q_R of the CH_4-hydrate formation during the stage II controlled by the clathration reaction. The reaction-rate constants $k_R = r_{i0}\rho_i B/\ln(f/f_d)$ are plotted versus $1/T$ in logarithmic scales in Figure 9a. With deuterated and hydrated ice samples, the slopes of the linear approximations yield $Q_R \approx 8.1 \pm 0.5$ and 9.5 ± 0.9 kcal/mol (0.35 and 0.4 eV), respectively. This difference is barely significant. A value of 5.6 kcal/mol (0.24 eV) was reported for the activation energy for the translational diffusion of water molecules in the quasi-liquid layer on the surface of ice (Mizuno and Hanafusa 1987),[24] which is clearly lower than the activation energies obtained from our experiments.

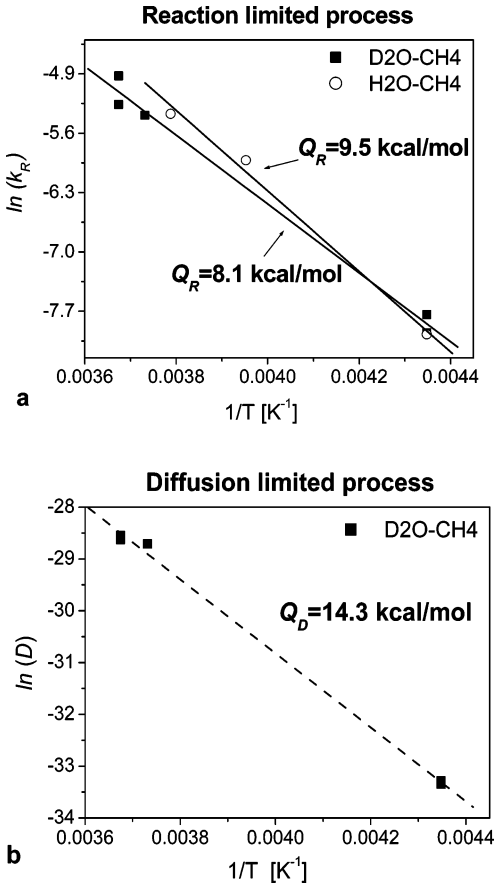

Figure 9. Activation energies of CH_4-hydrate formation deduced from the best-fit model parameters *B* and *D* (see Table 2) in reaction-limited (a) and diffusion-limited (b) approximations, for stages II and III, respectively. See notations in text.

If we assume that the stage I is followed by the diffusion-limited stage III, then the activation energy of the gas and water mass transport Q_D through the hydrate shells surrounding ice cores can be calculated from the estimates of the permeation coefficients given in Table 2. As shown in Figure 9b, we obtain $Q_D \approx 14.3 \pm 0.4$ kcal/mol (0.62 eV) for the CH_4-hydrate growth from deuterated ice. This is in perfect agreement with (Wang et al., 2002)[44] and indicates that in both cases similar kinetics of the gas-hydrate formation were observed. The activation energy of interstitial diffusion of water molecules in ice Ih is similar and amounts to 12.9 kcal/mol (0.56 eV) (Hondoh, 1992).[12] Whether this is an accidental agreement or indicative of the rate-limiting process of the clathration reaction must be considered as an open question.

The above analysis suggests that, at least in the beginning of the hydrate growth from ice powders, the process may be limited by the clathration reaction. However, further kinetic experiments of longer duration up to the reaction degrees of 90−100% performed with ice powders of different mean grain size are needed in order to reliably determine the rate-limiting steps and stage transitions in the kinetics of porous gas-hydrate formation.

5. Conclusion

A cryo field-emission scanning electron microscopy technique has recently been used to study porous gas hydrates grown on spherical ice grains. Although the molecular mechanisms of the formation of the submicron pores in hydrate crystallites are not properly understood, some common features of the submicron porous clathrates can be discerned in observations of their images. A general phenomenological description of the gas-hydrate formation from monodispersed ice powder is developed to describe the three predictable stages of the process. They are the initial stage I of the hydrate-film spreading over the ice surface and the two subsequent stages II and III of the porous hydrate layer growth limited by the clathration reaction (including the gas transport along the ice-hydrate interface) and by the diffusive gas/water mass transfer through the hydrate shells, respectively. This theory results in combined asymptotic eq 6 for stage I and its limiting form (eq 7) for stage II. A more sophisticated shrinking-core model taking account of the gas-hydrate growth into the macro-pore space of the sample (see eq 5) is suggested for stage III controlled (or influenced) by diffusion. Each rate-limiting step of the hydrate formation process and corresponding stages manifest themselves in different dependencies of the reaction degree on time and the mean initial ice grain size.

Further electron microscopic observations of porous gas hydrates are made, and several in situ kinetic neutron diffraction experiments on the CO_2- and CH_4-gas hydrate formation are performed and interpreted on the basis of model simulations. For the first time, neutron diffraction experiments were also performed with methane in hydrogenated samples. The structural isotopic differences between H_2O and D_2O are found to be negligible in terms of clathrate formation properties. Both reaction- and diffusion-limited approximations can equally well represent the kinetic data on the ice-to-hydrate conversion because of the limited observation periods. However, our analysis suggests that, at least in the beginning of the hydrate growth from ice powders, the process might be controlled by the clathration reaction itself. A clear difference between CO_2 and CH_4 concerning the reactivity is established with CO_2 reacting three times faster for similar excess pressures. A transient formation of the type-II CO_2 clathrate is observed together with the type-I structure growth. Comparable activation energies of CH_4-hydrate formation are found in deuterated and hydrogenated systems under the assumption of the reaction-limited process (stage II): 8.1 ± 0.5 and 9.5 ± 0.9 kcal/mol, respectively. In case of the diffusion-limited clathration (stage III), the activation energy in D_2O-ice powders is estimated as 14.3 ± 0.4 kcal/mol. Further studies and new data on the properties of the gas-ice-hydrate system are needed to reveal a more detailed picture of the porous clathrate hydrate growth on ice surfaces. Additional long-term experiments with ice samples of different grain size are necessary to better quantify the later stages of the clathration process. These experiments are well underway now.

Acknowledgment. The authors are grateful to Louis Melesi and Jean-Luc Laborier (ILL,Grenoble) for their help in preparing the high pressure equipment. We also thank Alice Klapproth and Georgi Genov (Göttingen) for discussions and help during sample preparation and data analysis. Loic Legagneux and Florent Dominé (LGGE, Grenoble) are gratefully acknowledged for performing the measurement of the specific surface area of the ice powder and porous gas hydrates. This work was supported by the DFG Grant Ku920/9-1 and through the BMBF Project 03G0553A in the framework of the German research initiative "Gas-Hydrate im Geosystem".

Appendix

Sample Structure Description and Diffusive Mass Transport through the Hydrate Shell. As suggested by Arzt (1982),[1] in a random dense packing without particle rearrangement, the

current coordination number Z can be expressed as a linear function of the relative hydrate shell radius $R_h = r_h/r_{i0}$

$$Z = Z_0 + C(R_h - 1) \quad \text{(A1)}$$

where the coordination number of the initial ice powder $Z_0 \sim 7$, and the slope of the random density function $C \sim 15.5$.

The normalized volume of a reference ice-hydrate particle schematically depicted in Figure 3a is directly related (Arzt, 1982)[1] to the reaction degree α

$$R_h^3 - \frac{Z_0}{4}(R_h - 1)^2(2R_h + 1) - \frac{C}{16}(R_h - 1)^3(3R_h + 1) = 1 + \alpha E \quad \text{(A2)}$$

The fraction s of the free hydrate surface area (in units of $4\pi r_h^2$) exposed to the ambient gas is (Arzt, 1982)[1]

$$s = 1 - \frac{Z_0}{2}\frac{R_h - 1}{R_h} - \frac{C}{4}\frac{(R_h - 1)^2}{R_h} \quad \text{(A3)}$$

The geometrical model (A1−A3) fully describes the sample packing development during the ice-to-hydrate conversion. The initial macroporosity of the ice powder ϵ_{m0} is directly linked to the packing parameters Z_0 and C in eq A1, the quantity $(1 - \epsilon_{m0})^{-1}$ being equal to the maximum normalized volume of the reference ice-hydrate particle, i.e., to the value of the left-hand side of eq A2 at $s = 0$ in eq A3. Accordingly, the current porosity ϵ_m and the normalized surface area of the macro-pore space are

$$\epsilon_m = \epsilon_{m0} - \alpha(1 - \epsilon_{m0})E, \quad S_m = sR_h^2 S_{i0}$$

The area of the spherical cap surface of radius r_h cut by one average contact from the truncated hydrate shell in Figure 3a can be calculated in two different ways:

$$2\pi r_h(r_h - r) = 4\pi r_h^2(1 - s)/Z$$

thus, yielding the distance r from the ice core center to an average contact plane

$$r = r_h\left[1 - \frac{2(1 - s)}{Z}\right]$$

The diffusive (permeation) resistance of the spherical sublayer 1 adjacent to the ice core (with internal and external radii r_i and r, respectively) per a unit of the core surface is conventionally (Crank, 1975)[7] written as

$$k_{D1}^{-1} = \frac{r_i^2}{\rho_i D}\left(\frac{1}{r_i} - \frac{1}{r}\right) \quad \text{(A4)}$$

In accordance with the insert in Figure 3a, let us locally replace component parts of the truncated convex sublayer 2 by segments of a concave spherical layer of the same thickness $r_h - r$ with the same areas of the concentric bounding surfaces of radii r_1 and r_2. This means that the ratios of the boundary areas must satisfy the following proportion:

$$\frac{r_1^2}{r_2^2} = \frac{sr_h^2}{r^2}$$

Because $r_2 - r_1 = r_h - r$, the latter relation directly leads to

$$r_1 = \frac{\sqrt{s}r_h(r_h - r)}{r - \sqrt{s}r_h}, \quad r_2 = \frac{r(r_h - r)}{r - \sqrt{s}r_h} \quad \text{(A5)}$$

The fraction ξ of the spherical layer which corresponds to the truncated hydrate layer 2 with the total free (outward) surface $4\pi r_h^2 s$ is

$$\xi = \frac{sr_h^2}{r_1^2} = \frac{(r - \sqrt{s}r_h)^2}{(r_h - r)^2} \quad \text{(A6)}$$

The diffusive resistance of the layer 2 is now presented in the form similar to eq A4

$$k_{D2}^{-1} = \frac{r_i^2}{\xi\rho_i D}\left(\frac{1}{r_1} - \frac{1}{r_2}\right) \quad \text{(A7)}$$

The sum of eqs A4 and A7

$$k_D^{-1} = k_{D1}^{-1} + k_{D2}^{-1}$$

after substitution of eqs A5 and A6 results in eq 5.

References and Notes

(1) Arzt, E. The influence of an increasing particle coordination on the densification of spherical powders. *Acta Metall.* **1982**, *30*, 1883−1890.

(2) Aya, K.; Yamane, K.; Yamada, N. Stability of clathrate hydrate of carbon dioxide in highly pressurized water. In *Fundamentals of Phase Change: Freezing, Melting, and Sublimation−1992 HTD*; Kroeger, P. E., Bayazitogu, Y., Eds.; The American Society of Mechanical Engineers: New York, 1992; Vol. 215, pp 17−22.

(3) Barrer, R. M.; Edge, A. V. J. Gas hydrates containing argon, krypton and xenon: kinetics and energetics of formation and equilibria. *Proc. R. Soc. London* A **1967**, *300*, 1−24.

(4) Berliner, R.; Popovici, M.; Herwig, K. W.; Berliner, M.; Jennings, H. M.; Thomas, J. J. Quasielastic neutron scattering study of the effect of water-to-cement ratio on the hydration kinetics of tricalcium silicate. *Cement Concrete Res.* **1998**, *28* (2), pp 231−243.

(5) Convert, P.; Hansen, T.; Oed, A.; Torregrossa, J. D20 high flux two axis neutron diffractometer. *ICNS '97 Proceedings*, *Physica B* **1998**, *241−243*, 195−197.

(6) Convert, P.; Hansen, T.; Torregrossa, J. The high-intensity two axis neutron diffractometer D20 − first results. *Proceedings of EPDIC6*, Budapest 1998, Materials Science Forum (Trans. Technol. Publications), 1999; Vols. 321−324, pp 314−319.

(7) Crank, J. *The Mathematics of Diffusion*, 2nd ed.; Clarendon Press: Oxford, 1975; Chapter 6.

(8) Fleyfel, F.; Devlin, J. P. Carbon dioxide clathrate hydrate epitaxial growth: spectroscopic evidence for formation of the simple Type-II CO_2 hydrate. *J. Phys. Chem.* **1991**, *95*, 3811−3815.

(9) Froment, G. F.; Bischoff, K. B. *Chemical Reactor Analysis and Design;* Wiley & Sons: New York, 1990.

(10) Fujii, K.; Kondo, W. Kinetics of hydration of tricalcium silicate. *J. Am. Ceram. Soc.* **1974**, *57*, 492−497.

(11) Henning, R. W.; Schultz, A. J.; Thien, Vu; Halpern, Y. Neutron diffraction sudies of CO_2 clathrate hydrate: formation from deuterated ice. *J. Phys. Chem.* **2000**, *104*, 5066−5071.

(12) Hondoh, T. Glide and climb processes of dislocations in ice. In *Physics and Chemistry of Ice*; Maeno, N., Hondoh, T., Eds.; Hokkaido University Press: Sapporo, Japan, 1992; pp 481−487.

(13) Hondoh, T.; Uchida, T. Formation process of clathrate air-hydrate crystals in polar ice sheets. *Teion Kagaku [Low-Temperature Science], Ser. A* **1992**, *51*, 197−212.

(14) Hwang, M. J.; Wright, D. A.; Kapur, A.; Holder, G. D. An experimental study of crystallization and crystal growth of methane hydrates from melting ice. *J. Inclusion Phenom.* **1990**, *8*, 103−116.

(15) Johari, G. P.; Jones, S. J. Dielectric properties of polycrystalline D2O ice Ih. *Proc. R. Soc. London* **1976**, *A349*, 467−495.

(16) Johari, G. P.; Jones, S. J. The orientation polarization in hexagonal ice parallel and perpendicular to the *c*-axis. *J. Glaciol.* **1978**, *21*, 259−276.

(17) Klapproth, A. Ph.D. Thesis, Universität Göttingen. Strukturuntersuchungen an Methan- und Kohlenstoffdioxid-Clathrat-Hydraten, 2002.

(18) Klapproth, A.; Goreshnik, E.; Staykova, D.; Klein, H.; Kuhs, W. F. Structural Studies of Gas Hydrates. *Can. J. Phys.* **2003**, *81*, 503−518.

(19) Kobayashi, I.; Ito, Y.; Mori, Y. H. Microscopic observations of clathrate-hydrate films formed at liquid/liquid interfaces. I. Morphology of hydrate films. *Chem. Eng. Sci.* **2001**, *56*, 4331−4338.

(20) Kuhs W. F.; Klapproth, A.; Gotthardt, F.; Techmer, K.; Heinrichs, T. The formation of meso- and macroporous gas hydrates. *Geophys. Res. Lett.* **2000**, *27* (18), 2929−2932.

(21) Larson, A. C.; B. Von Dreele, R. Report No. LAUR, 1990, pp 86−748.

(22) Legagneux, L.; Cabanes, A.; Dominé, F. Measurement of the specific surface area of 176 snow samples using methane adsorption at 77K. *J. Geophys. Res.* **2002**, *107*, 4335−4349.

(23) Levenspiel, O. *Chemical Reaction Engineering*; Wiley & Sons: New York, 1999.

(24) Mizuno, Y.; Hanafusa, N. Studies of surface properties of ice using nuclear magnetic resonance. *J. Phys., Colloque C1, Suppl. N3* **1987**, *48*, C1−511-C1−517.

(25) Mori, Y. H. Clathrate hydrate formation at the interface between liquid CO_2 and water phases: a review of rival models characterizing "hydrate films". *Energy Convers. Manage.* **1998**, *39* (15), 1537−1257.

(26) Mori, Y. H.; Mochizuki, T. Mass transport across clathrate hydrate films − a capillary permeation model. *Chem. Eng. Sci.* **1997**, *52* (20), 3613−3616.

(27) Moudrakovski, I. L.; Sanchez, A. A.; Ratcliffe, C. I.; Ripmeester, J. A. Nucleation and growth of hydrates on ice surfaces: new insights from ^{129}Xe NMR experiments with hyperpolarized xenon. *J. Phys. Chem. B* **2001**, *105*, 12338−12347.

(28) Ohmura, R.; Kashiwazaki, S.; Mori, Y. H. Measurements of clathrate-hydrate film thickness using laser interferometry. *J. Cryst. Growth* **2000**, *218*, 372−380.

(29) Pietrass, T.; Gaede, H. C.; Bifone, A.; Pines A.; Ripmeester, J. A. Monitoring xenon clathrate hydrate formation on ice surfaces with optically enhanced ^{129}Xe NMR. *J. Am. Chem. Soc.* **1995**, *117*, 7520−7525.

(30) Salamatin, A. N.; Hondoh, T.; Uchida, T.; Lipenkov, V. Ya. Post-nucleation conversion of an air bubble to clathrate air-hydrate crystal in ice. *J. Cryst. Growth* **1998**, *193*, 197−218.

(31) Salamatin, A. N.; Kuhs W. F. Formation of porous gas hydrates. *Proc. 4th Int. Conf. Gas Hydrates* **2002**, 766−770.

(32) Sloan, E. D., Jr. *Clathrate Hydrates of Natural Gases*, 2nd ed.; Marcel Dekker Inc.: New York, 1998.

(33) Sloan, E. D., Jr.; Fleyfel, F. A molecular mechanism for gas hydrate nucleation from ice. *AIChE J.* **1991**, *37*, 1281−1292.

(34) Staykova, D. K.; Hansen, T.; Salamatin, A. N.; Kuhs, W. F. Kinetic diffraction experiments on the formation of porous gas hydrates. *Proc. 4th Int. Conf. Gas Hydrates* **2002**, 537−542.

(35) Stern, L. A.; Hogenboom, D. L.; Durham, W. B.; Kirby, S. H.; Chou, I.-M. Optical-cell evidence for superheated ice under gas-hydrate-forming conditions. *J. Phys. Chem. B* **1998**, *102*, 2627−2632.

(36) Suess, E.; Bohrmann, G.; Rickert, D.; Kuhs, W. F.; Torres, M.; Tréhu, A.; Linke, P. Properties and fabric of near-surface methane hydrates at Hydrate Ridge, Cascadia Margin. *Proc. 4th Int. Conf. Gas Hydrates* **2002**, 740−744.

(37) Sugaya, M.; Mori, Y. H. Behavior of clathrate hydrate formation at the boundary of liquid water and fluorocarbon in liquid or vapor state. *Chem. Eng. Sci.* **1996**, *51* (13), 3505−3517.

(38) Takeya, S.; Hondoh, T.; Uchida, T. In situ observations of CO_2 hydrate by X-ray diffraction. *Ann. NY Acad. Sci.* **2000**, *912*, 973−982.

(39) Takeya, S.; Shimada, W.; Kamata, Y.; Ebinuma, T.; Uchida, T.; Nagao, J.; Narita, H. In situ X-ray diffraction measurements of the self-preservation effect of CH_4 hydrate. *J. Phys. Chem. A* **2001**, *105*, 9756−9759.

(40) Uchida, T.; Hondoh, T.; Mae, S.; Duval, P.; Lipenkov, V. Ya. In-situ observations of growth process of clathrate air-hydrate under hydrostatic pressure. In *Physics and Chemistry of Ice*; Maeno, N., Hondoh, T., Eds., Hokkaido University Press: Sapporo, Japan, 1992; pp 121−125.

(41) Uchida, T.; Hondoh, T.; Mae, S.; Duval, P.; Lipenkov, V. Ya. Effects of temperature and pressure on transformation rate from air bubbles to air-hydrate crystals in ice sheets. *Ann. Glaciol.* **1994**, *20*, 143−147.

(42) Uchida, T.; Kawabata, J. Observations of water droplets in liquid carbon dioxide. *Proc. MARIENV '95 Conf.* **1995**, 906−910.

(43) van der Waals, J. H.; Platteeuw, J. C. Clathrate solutions. *Adv. Chem. Phys.* **1959**, *2* (1), 1−57.

(44) Wang, X.; Schultz A. J.; Halpern, Y. Kinetics of ice particle conversion to methane hydrate. *Proc. 4th Int. Conf. Gas Hydrates* **2002**, 455−460.

(45) Warzinski, R. P.; Lynn, R. J.; Holder, G. D. The impact of CO_2 clathrate hydrate on deep ocean sequestration of CO_2. *Ann. NY Acad. Sci.* **2000**, *912*, 226−234.